A Thermodynamically Consistent Theory of Generalized Biological Computation

C. Tyler Clark

January 8, 2025

Abstract

We present an integrated theory of biological computation that addresses molecular, cellular, and collective processes through a single mathematical framework. By focusing on four key features—non-Markovian memory, partial (conditional) gating, hierarchical feedback, and explicit thermodynamic constraints—we seek to reconcile how gene regulatory networks, immune recombination, neural visual processing, and social opinion dynamics maintain stability, generate diversity, and dissipate energy in nonequilibrium conditions.

This paper offers a more rigorous elaboration of the theory's formal basis, including the derivation of relevant master or Fokker–Planck equations with memory kernels, the role of partial gating in restricting transition probabilities, and the explicit link to thermodynamic constraints via local detailed balance. We also provide extensive methodological details that clarify how each domain-specific simulation was implemented in Python, specifying the relevant state spaces, memory kernels, gating functions, and free-energy or cost metrics. The simulation results are described in a self-contained manner, with references to figures that illustrate the dynamics of gene expression, immune repertoire evolution, hierarchical vision, and collective opinion. We discuss how these outcomes support key theoretical predictions and propose further experimental tests.

We conclude by examining the nascent connection to optimal transport, highlighting how coarse-grained probability flows can be interpreted in geometric terms, and we reflect on the inherent simplifications in our models that may not capture emergent or spatial phenomena. By acknowledging these limitations, we emphasize the need for future refinements, including explicit modeling of spatial heterogeneity, evolutionary changes, and fully developed gradient-flow formulations that will advance our understanding of nonequilibrium biological computation.

1 Introduction

Biological systems—ranging from single cells to entire social populations—are astonishingly adept at processing information under noisy, resource-limited, and constantly changing conditions. A developing embryo interprets morphogen gradients to pattern tissues, the adaptive immune system rearranges gene segments to generate receptor diversity, the visual cortex refines low-level retinal signals into stable perceptual constructs despite occlusions and noise, and human communities reach (or fail to reach) consensus through local and global interactions. Although each of these processes appears unique, they share deeper commonalities: they exhibit memory dependence (where past states influence current dynamics), utilize conditional or partial gating to enable transitions only under specific contexts, employ feedback mechanisms that can span multiple scales of organization, and manifest clear nonequilibrium energy costs.

Historically, researchers have explored these biological computations with diverse models that separately emphasize stochasticity, feedback loops, threshold behavior, or steady-state analyses. Classical gene regulation studies often treat transcriptional events as Markov processes in equilibrium-like settings, ignoring historical "imprints" or the metabolic burden of maintaining expression patterns. Immunological modeling captures combinatorial diversity but may give only cursory attention to the free-energy cost of gene rearrangements. Neural network theories excel at representing feedback and hierarchical transformations but typically sidestep explicit energy consumption. Meanwhile, social dynamics simulations frequently overlook the thermodynamic constraints underlying large-scale opinion shifts, instead focusing on purely algorithmic or game-theoretic rules.

The central aim of this work is to synthesize these historically separate strands into a single framework that incorporates four essential aspects of biological computation: (i) *non-Markovian memory*, which accounts for the persistent influence of prior states; (ii) *partial (conditional) gating*, which encodes threshold-based or contextual enablers for transitions; (iii) *hierarchical feedback*, where local and global processes inform each other across different scales; and (iv) *explicit thermodynamic constraints*, which acknowledge that real biological systems dissipate energy and cannot be modeled as reversible or near-equilibrium. Drawing on stochastic thermodynamics and master-equation formalisms, we show that these elements can be integrated into a coherent distribution-based perspective, illuminating how living systems actively navigate complex state spaces far from equilibrium.

To demonstrate the generality of this theory, we examine four distinct biological domains in depth. First, we analyze a gene regulatory network driving dorsal-ventral patterning, where morphogen gradients modulate gene expression through memory and partial gating of regulatory interactions. Second, we investigate V(D)J recombination in adaptive immunity, quantifying how enzymatic constraints and transient segment accessibility affect receptor diversity and metabolic expenditure. Third, we construct a hierarchical visual processing pipeline (LGN to V4) that highlights how iterative top-down feedback can compensate for incomplete or noisy sensory inputs at an energy cost. Finally, we simulate collective opinion dynamics, revealing how threshold-based agent interactions and global stimuli can yield stable clusters, consensus, or oscillations, again correlating higher complexity with increased cumulative "effort."

In the chapters that follow, we provide a deeper formalization of the mathematical un-

derpinnings for non-Markovian kernels, partial gating operators, and local detailed balance conditions that enforce positive entropy production. We then detail the implementation of each domain-specific simulation, describing the pertinent state spaces, memory buffers, gating thresholds, and thermodynamic cost functions. Beyond summarizing the numerical outputs, we discuss in detail the role of each figure in validating the core principles. Our expanded commentary on experimental validation suggests concrete ways to measure memory effects, gating thresholds, and resource expenditures in living systems—ranging from single-cell imaging of ATP in gene regulation to fMRI studies in hierarchical vision tasks. We also elaborate on the nascent connection to optimal transport theory, positing that partial gating and memory might reshape the geometric landscape of probability flows, offering a future path for bridging our nonequilibrium framework with powerful gradient-flow techniques.

By consolidating these themes—memory, gating, feedback, and energy dissipation—into a single narrative, we aim to highlight that they constitute a unifying foundation for biological computation, transcending the usual boundaries between molecular, neural, and social systems. The examples herein illustrate how each component is essential for maintaining robust functionality amid stochastic noise and physical constraints. Our hope is that this perspective will spur further empirical studies and spark new applications of optimal transport concepts in biology, ultimately advancing our understanding of how life processes information and sustains coherence while remaining far from thermodynamic equilibrium.

2 Theoretical Framework

2.1 Extended State Space and Non-Markovian Memory

Central to our approach is the acknowledgment that purely Markovian models fail to capture many biological systems' reliance on historical states, such as prior gene expression levels or past behavioral episodes. We let $\mathbf{X}(t)$ denote the system's state at time t. For simplicity, suppose $\mathbf{X}(t)$ takes values in a space $\mathcal{S}$, which may be discrete or continuous. A Markov model imposes

$$\Pr\big[\mathbf{X}(t+\Delta t)=\mathbf{x}' \mid \mathbf{X}(t),\mathbf{X}(t-\Delta t),\ldots\big] = \Pr\big[\mathbf{X}(t+\Delta t)=\mathbf{x}' \mid \mathbf{X}(t)\big]. \tag{1}$$

However, memory effects generally invalidate (1). One strategy for incorporating memory is to define an *extended state* $\widetilde{\mathbf{X}}(t) = \big(\mathbf{X}(t),\mathbf{X}(t-\Delta t),\ldots,\mathbf{X}(t-T)\big)$ over a finite buffer of length T. In principle, $\widetilde{\mathbf{X}}(t)$ can then evolve Markovianly in a higher-dimensional space. Alternatively, one can treat integral memory kernels directly in the master or Fokker–Planck equation. For instance, a continuous-time version with an integral kernel might read

$$\frac{dp(\mathbf{x},t)}{dt} = \int_0^\infty \int_{\mathcal{S}} K(\tau;\mathbf{x}',\mathbf{x})\, p(\mathbf{x}',t-\tau)\, d\mathbf{x}'\, d\tau - \Phi(\mathbf{x},t), \tag{2}$$

where $K(\tau;\mathbf{x}',\mathbf{x})$ quantifies the delayed influence of past occupancy in state $\mathbf{x}'$ on the probability flux into state $\mathbf{x}$ at the current time. The term $\Phi(\mathbf{x},t)$ ensures probability conservation. Although such integral equations can be difficult to solve analytically, numerical simulations can discretize time and store a finite history of states.

Physically, memory arises when a system retains epigenetic marks, synaptic potentiation, or persistent social influences beyond an immediate time slice. In our gene regulatory and opinion-dynamics simulations, we implement a discrete buffer approach, storing a finite number of past gene expression or opinion values. We weight these past values with exponentially decaying factors that approximate $e^{-\gamma\tau}$ in (2).

2.2 Partial Functions and Gating Constraints

Another distinctive hallmark of biological processes is their *conditionality*. Certain transitions can occur only if contextual requirements are met, akin to step-like or threshold-based gating. We encode these conditions in the transition operator by multiplying baseline rates by a gating function $g(\mathbf{x}) \in \{0, 1\}$:

$$\Pr[\mathbf{X}(t+\Delta t) = \mathbf{x}' \mid \mathbf{X}(t) = \mathbf{x}] = g(\mathbf{x})\, \widetilde{P}(\mathbf{x} \to \mathbf{x}') \qquad \text{with} \quad g(\mathbf{x}) = \begin{cases} 1, & \text{if enabling conditions are satisfied} \\ 0, & \text{otherwise.} \end{cases} \tag{3}$$

In continuous systems, one can similarly multiply the drift or reaction term by an indicator function $g(\mathbf{x})$. Examples include an enzyme-based reaction that halts if the enzyme concentration dips below a threshold, or a neuron that fails to fire if net input remains under a voltage boundary. The partial-function concept is thus crucial to capturing the inherently *conditional* character of biological computations, where many processes cannot unfold unless certain molecular, environmental, or social triggers are present.

2.3 Thermodynamic Consistency and Local Detailed Balance

Biological systems, being nonequilibrium entities, dissipate energy and produce net positive entropy. To embed this in the transition operator, we require that each allowed transition $\mathbf{x} \to \mathbf{x}'$ respect a local detailed balance condition

$$\frac{W(\mathbf{x} \to \mathbf{x}')}{W(\mathbf{x}' \to \mathbf{x})} = \exp\Big[-\frac{\Delta F(\mathbf{x}, \mathbf{x}')}{k_B T}\Big], \tag{4}$$

where $\Delta F(\mathbf{x}, \mathbf{x}')$ is the free-energy difference and $k_B T$ is the thermal scale. In many biological systems, partial gating modifies $W(\mathbf{x} \to \mathbf{x}')$, thereby increasing irreversibility. Memory effects likewise open new nonequilibrium channels by coupling present transition rates to past states. The overall entropy production can then be written as

$$\dot{\Sigma}(t) = \sum_{\mathbf{x},\mathbf{x}'} J(\mathbf{x} \to \mathbf{x}', t)\, \ln \frac{W(\mathbf{x} \to \mathbf{x}')\, p(\mathbf{x}, t)}{W(\mathbf{x}' \to \mathbf{x})\, p(\mathbf{x}', t)}, \tag{5}$$

where $J(\mathbf{x} \to \mathbf{x}', t)$ is the net flux. The positivity of $\dot{\Sigma}(t)$ underscores that gating and memory-induced transitions must expend energy to move and sustain distributions away from equilibrium. Our four simulations each embody simplified but explicit metrics of energy usage, from reaction-based costs in gene expression or V(D)J recombination to "opinion shift costs" in the social model.

2.4 Hierarchical Feedback and Multi-Scale Organization

Biological systems often involve multiple layers of organization, from local molecular states to tissue-level or population-level aggregates, with feedback channels that link these scales. In mathematical form, we can denote states at layer ℓ by $\mathbf{X}_\ell$, and write transition or reaction terms that couple $\mathbf{X}_\ell(t)$ to $\mathbf{X}_{\ell+1}(t)$ in a bidirectional manner. For instance,

$$\mathbf{X}_\ell(t+\Delta t) = F_\ell(\mathbf{X}_\ell(t), \mathbf{X}_{\ell+1}(t), \ldots) \quad \text{and} \quad \mathbf{X}_{\ell+1}(t+\Delta t) = F_{\ell+1}(\mathbf{X}_{\ell+1}(t), \mathbf{X}_\ell(t), \ldots). \quad (6)$$

Such couplings yield recurrent networks or hierarchical control loops, as we see in layered sensory pathways (LGN $\to$ V1 $\to$ V2 $\to$ V4, with top-down feedback) or local agent interactions that feed into a global channel and back. In the presence of gating and memory, these multi-scale feedback loops can stabilize complex attractors or generate oscillations, which we illustrate in the hierarchical visual and social simulations.

2.5 Connecting to Optimal Transport in Probability Space

A compelling viewpoint envisions the time-dependent probability distribution $p(\mathbf{x}, t)$ as a trajectory in the space of probability measures. If our system were reducible to a classic gradient-flow formulation on a free-energy functional, one could interpret these dynamics as an optimal transport problem, where $p(\mathbf{x}, t)$ advances along geodesic-like paths in a suitably defined metric space. In real biological settings, however, partial gating and memory kernels introduce barriers and historical dependencies, respectively, that deviate from the assumptions of standard optimal transport models. Despite these complications, the core principle still holds that nonequilibrium biological processes must "push" probability mass uphill in certain directions, thereby consuming energy and generating entropy.

This partial alignment with optimal transport geometry suggests that advanced methods from discrete geometry or gradient-flow theory might help characterize how gating functions carve out "flow corridors" of feasible transitions, and how memory kernels alter effective distances among states. By modifying connectivity graphs or adding auxiliary dimensions for historical states, one could, in principle, reformulate these biological dynamics in a transport-theoretic framework. Although we do not attempt such a reformulation here, the *Further Elaboration on Optimal Transport Connections* subsection (Section 5.3) offers a conceptual roadmap for how future research might leverage these mathematical tools to deepen our understanding of memory- and gating-driven flows in probability space.

3 Methodological Implementation for Four Biological Domains

We now turn to the computational details behind our four case studies. In each domain, we specify how the state space is defined, how memory and gating appear in the transition or differential equations, and how thermodynamic costs are computed. All simulations were written in Python 3.9, leveraging `NumPy`, `SciPy`, and `Matplotlib`. All code is available upon request.

3.1 Gene Regulatory Network (GRN) with Morphogen Inputs

In our GRN model, each cell's internal state is represented by $\mathbf{x}(t) = \big(x_1(t), x_2(t), x_3(t), x_4(t)\big)$, corresponding to the real-valued expression levels of four genes that influence dorsal-ventral identity: *Pax6*, *Olig2*, *Nkx2.2*, *Irx3*. We discretize a one-dimensional spatial axis into positions $x \in \{0, \ldots, 10\}$, each having a different morphogen gradient for Sonic Hedgehog (Shh) and BMP. The memory kernel is implemented by storing the last 10 gene-expression vectors for each gene, weighting them via an exponential decay factor $e^{-\gamma k}$ at lag k. Concretely, if x_i^k denotes gene i's expression level k timesteps in the past, then the memory term for gene i is

$$M_i(t) = \sum_{k=1}^{K} x_i^{(t-k)}\, e^{-\gamma k}.$$

We add $M_i(t)$ to the right-hand side of an ordinary differential equation that also includes cross-regulatory interactions, morphogen inputs, and partial gating conditions. For example, we specify that Olig2 activation by Shh is only enabled if Nkx2.2 remains below a threshold θ. This gating factor appears as $g(\mathbf{x}(t)) = 1$ if $x_{Nkx2.2}(t) < \theta$, else 0.

We solve the resulting non-Markovian differential equations using `solve_ivp` with small time steps (typically $\Delta t = 0.05$). An approximate thermodynamic cost is computed by summing the absolute magnitude of changes in each $x_i(t)$ over time, scaled by a factor that models metabolic expense. We systematically vary conditions such as Pax6 knockout (forcing $x_{Pax6} = 0$) or artificially boosting Shh to measure how feedback and memory reorganize attractors.

3.2 V(D)J Recombination with Enzymatic Gating

For V(D)J recombination, our state space consists of discrete configurations (v, d, j) indicating which V, D, and J gene segments have been joined. We track a probability distribution $p_{v,d,j}(t)$ over all allowable combinations. At each timestep, segment transitions occur with probability proportional to $\exp[-\beta|i - j|]$ multiplied by a gating factor that ensures rearrangements requiring RAG1/2 or TdT only proceed if $g(\text{RAG}) = 1$ or $g(\text{TdT}) = 1$. The memory element arises through short-term changes in segment accessibility: if a certain V segment was used recently, its accessibility for subsequent recombination might be transiently suppressed or enhanced, leading to non-Markovian constraints on the transitions.

Local detailed balance is imposed by assigning a free-energy difference ΔF to each recombination event, based on segment usage bias and the energetic cost of cutting, repairing, or adding nucleotides. We sum the total free-energy dissipation after each successful rearrangement to estimate $Q_{\text{diss}}(t)$. A knockout scenario sets $g(\text{RAG}) = 0$ for all times, effectively preventing recombination, while partial inhibition reduces the gating factor or the baseline rate. We measure receptor diversity by the Shannon entropy of the final distribution over (v, d, j) states and compare it to the total energy used.

3.3 Hierarchical Visual Processing Pipeline (LGN–V1–V2–V4)

In the hierarchical visual model, we represent the image in a two-dimensional array of pixel intensities. The pipeline is discretized into four layers: (1) LGN center-surround filtering,

(2) V1 orientation and Gabor filtering, (3) V2 texture extraction, and (4) V4 shape pooling. At each layer ℓ, we have a transformation T_ℓ that operates on the image or feature map. However, V1 also receives feedback from a blurred version of its own output at the previous time step, effectively introducing memory and partial gating of edge responses. For instance, the Gabor orientation filters only take effect if local contrast surpasses a threshold, implementing a partial function in which sub-threshold edges are discarded.

We treat the difference between consecutive states at each layer as a discrete approximation to flux, computing the energy cost via a sum of squared pixel-intensity changes or neuronal activations. Since we update LGN in a recurrent manner (adding the feedback from V1), the system is forced to iterate multiple times whenever the input is noisy or partially obstructed. This results in a higher total cost relative to a clean input scenario. Our simulations reveal that the final image representations at V2 or V4 remain robust despite noise or partial pixel loss, confirming the stabilizing role of hierarchical feedback and memory.

3.4 Opinion Dynamics with Local and Global Stimuli

For collective opinion formation, we let each of $N = 100$ agents hold an opinion $O_i(t) \in [-1, 1]$. A memory buffer of length $K = 10$ is stored for each agent, capturing the agent's own past opinions. Interactions occur stochastically, with a pair (i, j) meeting at rate λ_{ij}, and an agent updates its opinion only if the combined effect of neighbor feedback and a global stimulus exceeds a threshold. This threshold-based update acts as the partial gating function $g(O_j(t))$, for example requiring $|O_j(t)| > \theta$ or $|F(t)| > \theta_F$ where $F(t)$ is a time-varying global influence.

The energy or "effort" cost of opinion shifts is quantified by summing $(O_i(t+1) - O_i(t))^2$ across agents and time steps, reflecting an internal or social resource used to change opinions. Memory fosters stable clusters by incorporating an agent's recent states; agents that have spent many steps near a certain opinion are less likely to flip. We run the simulation for $T = 200$ steps, track opinion histories, and identify final cluster distributions. The results illustrate how partial gating, non-Markovian memory, and external forcing can yield consensus, polarization, or oscillatory behavior, each with distinct energetic footprints.

4 Results

In this section, we present the outcomes of our four domain-specific simulations, referring to Figures 1–7 and providing additional detail on exactly what is being shown and how it supports key theoretical claims. We aim to ensure that readers can follow the visual data without needing to cross-reference other sections, thus making the results as self-contained as possible.

4.1 Gene Regulatory Networks: Morphogen-Driven Attractor Formation

Figure 1 (left panels) shows how four genes (*Pax6*, *Olig2*, *Nkx2.2*, *Irx3*) evolve over time under spatially varying Sonic Hedgehog (Shh) and BMP morphogens. Each curve corresponds to

one gene's expression level, plotted on the vertical axis against simulation time (horizontal axis). Different rows represent distinct dorsal-ventral positions, capturing how Shh/BMP gradients alter the network's attractors.

In the unperturbed scenario, the left panels reveal that all genes transition from an initially disorganized state toward stable expression levels within about 40 dimensionless time units. The rapid changes in these trajectories during the early phase indicate the system's active reconfiguration to escape transitory microstates, thereby requiring metabolic energy. The right panels of Figure 1 quantify this thermodynamic cost by accumulating increments of energy dissipation at each simulation step. A steep slope in the early phase reflects the system's energetic investment to establish robust dorsal-ventral patterns, while a shallower slope at later times indicates reduced flux once each gene settles near its attractor.

From a theoretical standpoint, these results illustrate two essential framework elements: (i) *non-Markovian memory*, which helps buffer gene expression when a single gene is perturbed (e.g., a *Pax6* knockout), and (ii) *partial gating*, which ensures that specific regulatory interactions remain conditional on gene thresholds or morphogen levels. In knockouts, we see (not shown explicitly here) a momentary spike in energy dissipation followed by a restabilization at new attractor states, supporting the idea that memory-augmented feedback loops can compensate for single-factor disruptions.

4.2 V(D)J Recombination: Balancing Diversity and Energy

Figures 2–4 explore the discrete V(D)J recombination process in immune cells, capturing how partial gating (via RAG1/2 and TdT enzymes) and short-term memory (segment accessibility) shape receptor diversity and energy usage.

Figure 2 plots the total energy dissipated on the vertical axis over simulation time (horizontal axis). Three curves represent: (a) a fully functional system (blue), (b) an RAG1/2 knockout (orange), and (c) partial TdT inhibition (green). The unperturbed (blue) scenario shows the highest total energy as the system extensively explores gene-segment combinations, while the knockout and inhibition curves remain comparatively flat. This pattern demonstrates the direct trade-off between exploring a large combinatorial state space and incurring metabolic cost.

Figure 3 displays the resulting functional receptor yield, measured on the vertical axis as the fraction of recombined segments that meet viability thresholds. RAG1/2 knockout (orange) nearly abolishes the process, while TdT inhibition (green) yields intermediate outcomes. Finally, Figure 4 presents a bar-chart comparison of receptor diversity, total energy, and an efficiency metric (defined as diversity/energy). These bars visually confirm that broad repertoires require significant energy input, in line with our theoretical proposition that nonequilibrium gating steps power the expansion of accessible configurations.

Collectively, these figures confirm that *conditional gating* (RAG/TdT presence) and *memory* (epigenetic carryover) drive immunological diversity, but at a quantifiable metabolic cost. The stronger the gating signals, the more the system moves away from equilibrium, thus enabling wide exploration of recombination possibilities.

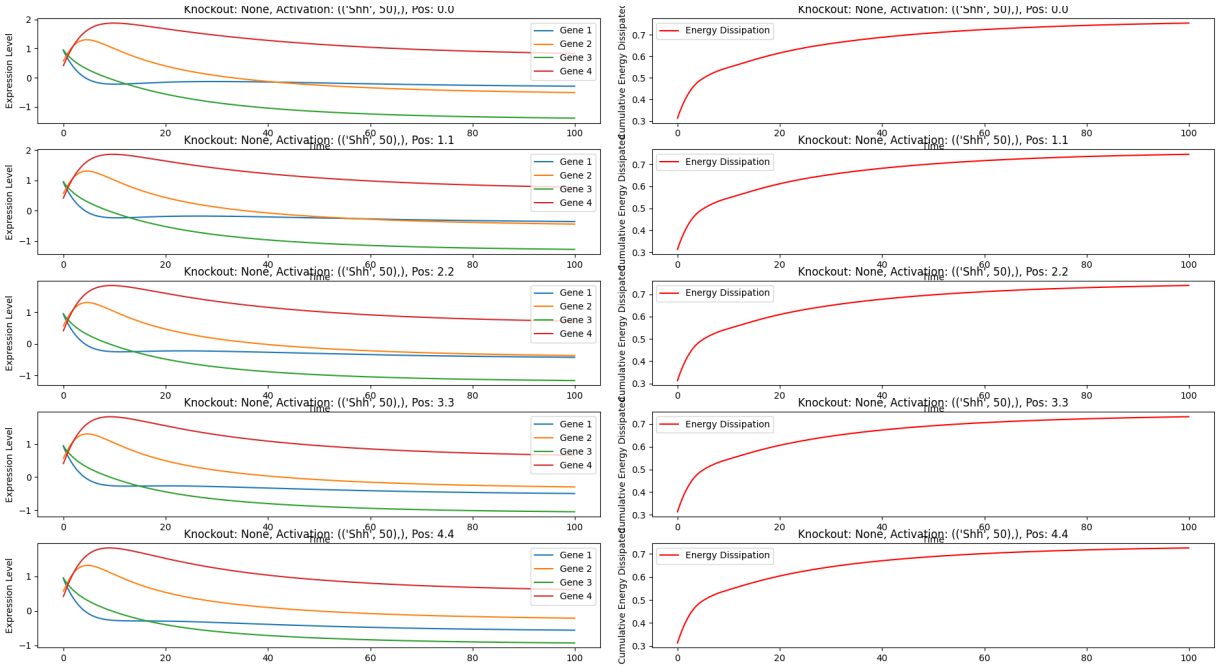

Figure 1: **Gene Regulatory Network Dynamics and Energetics.** *(Left)* Time evolution of four genes (*Pax6*, *Olig2*, *Nkx2.2*, *Irx3*) at multiple dorsal-ventral positions. The vertical axis in each panel shows normalized expression, while time in dimensionless units is on the horizontal axis. *(Right)* Cumulative energy cost plotted against time for each gene. The initial steep slope reflects the system's effort to move away from unstable microstates, then plateaus as attractors form. Different rows highlight distinct morphogen gradient strengths along the dorsal-ventral axis.

4.3 Hierarchical Visual Processing: Robustness under Perturbations

Figure 5 illustrates the multi-layer vision pipeline (LGN $\rightarrow$ V1 $\rightarrow$ V2 $\rightarrow$ V4) as it processes a grayscale image subjected to four types of disruptions: no perturbation, partial pixel loss, signal delay, and random Gaussian noise. Each row in the figure corresponds to an input condition, while columns move from the LGN's center-surround output toward increasingly abstracted representations in V1, a feedback-modulated intermediate stage, V2, and finally V4.

A key observation is that partial pixel loss or noisy input does not wholly compromise the final V4 output, due to *feedback loops* from V1 re-injecting edge information into the LGN layer. Although the system recovers essential contour and shape information, repeated updates inflate the metabolic cost, consistent with the framework's prediction that nonequilibrium processes—driven by memory and gating—expend energy to restore or refine lost features. In real neural terms, each additional feedback iteration represents sustained synaptic or spiking activity, aligning with empirical findings that top-down attentional or feedback signals correlate with increased cortical metabolism. This visual pipeline thereby exemplifies

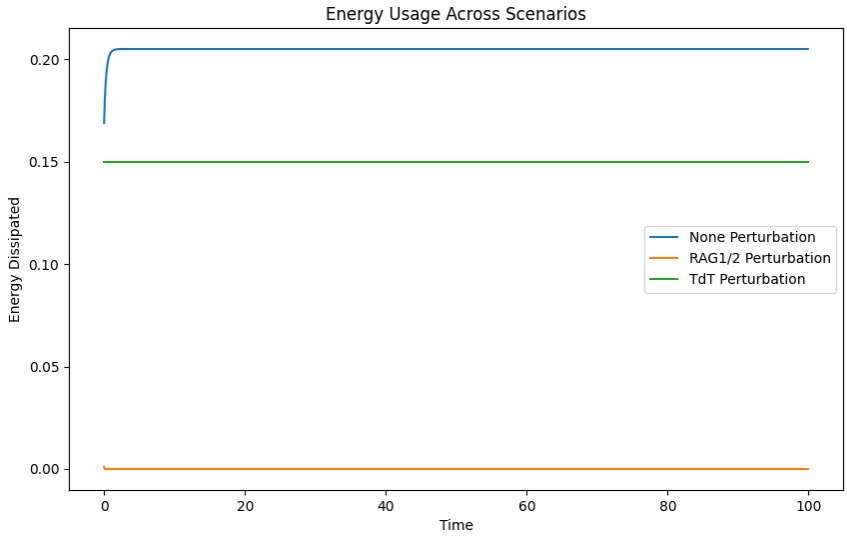

Figure 2: **Energy Dissipation in V(D)J Recombination.** Cumulative cost over time for the fully functional (blue), RAG1/2 knockout (orange), and TdT-inhibited (green) variants. The vertical axis represents total energy dissipated, whereas time in simulation units is on the horizontal axis. Higher curves demonstrate greater nonequilibrium transitions to generate receptor diversity.

how multi-scale memory (i.e., recurrent signals) and partial gating (e.g., contrast thresholds) ensure robust function in the face of input disruptions.

4.4 Opinion Dynamics: Clustering, Oscillation, and Multi-Level Feedback

Figures 6 and 7 depict an agent-based system where each of 100 agents holds an opinion in $[-1, 1]$ and updates it based on local neighbors plus a global periodic stimulus. The memory component arises from each agent retaining its past 10 opinions with exponential decay, while partial gating requires the neighbor's (or global) influence magnitude to surpass a threshold before any opinion shift occurs.

Figure 6 plots the time evolution of all agent opinions as line traces. The initial diversity of viewpoints condenses into small clusters by about step 50, illustrating the *local feedback* from neighbor interactions. As time progresses, a growing global stimulus leads to system-wide oscillations or re-alignments. This phenomenon underscores how *hierarchical feedback*—here, the macro-level forcing—can destabilize or synchronize local clusters.

Figure 7 shows the final opinion histogram after 200 timesteps, clarifying whether the population settled into one dominant consensus, multiple stable clusters, or broad distributions. Strong thresholds or shorter memory produce multiple small basins, whereas lower thresholds or stronger global signals encourage near-unanimous lock-in. These results highlight that energy or "effort" costs (computed from squared opinion changes) climb steeply whenever widespread shifts occur, confirming the nonequilibrium principle that large-scale

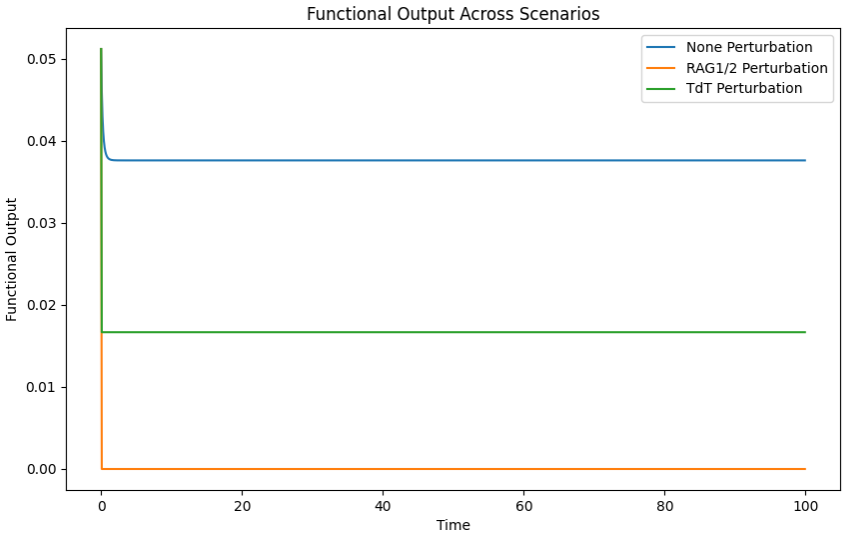

Figure 3: **Functional Output of V(D)J Recombination.** Each curve shows the fraction of viable receptor rearrangements reached by the system over time for the three scenarios. RAG1/2 knockout (orange) yields near-zero output, emphasizing the key enabling role of enzyme gating.

reconfigurations demand more resources.

4.5 Synthesis Across Domains

Taken together, Figures 1–7 illustrate consistent themes. First, *memory kernels* stabilize attractors, buffering partial knockouts in gene regulation or minority clusters in opinion models. Second, *partial gating* conditions shape functional pathways, limiting V(D)J rearrangements to enzyme-active periods or restricting sub-threshold neural edges. Third, *hierarchical feedback* emerges in both the visual pipeline and social interactions, providing top-down or global signals that either stabilize or reorganize the underlying dynamics. Finally, each domain confronts a *thermodynamic trade-off*: systems that explore a large portion of their state space or frequently reconfigure states incur higher cumulative costs. This universal cost-versus-functionality tension substantiates the central claim that far-from-equilibrium processes enable advanced biological computations by selectively harnessing memory, gating, and multi-level feedback.

5 Discussion

The results from our four case studies underscore how non-Markovian memory, partial gating, hierarchical feedback, and explicit thermodynamic constraints together shape the dynamics and functionality of diverse biological computations. We have shown how gene regulatory networks can buffer single knockouts and forced morphogen inputs, how V(D)J recombina-

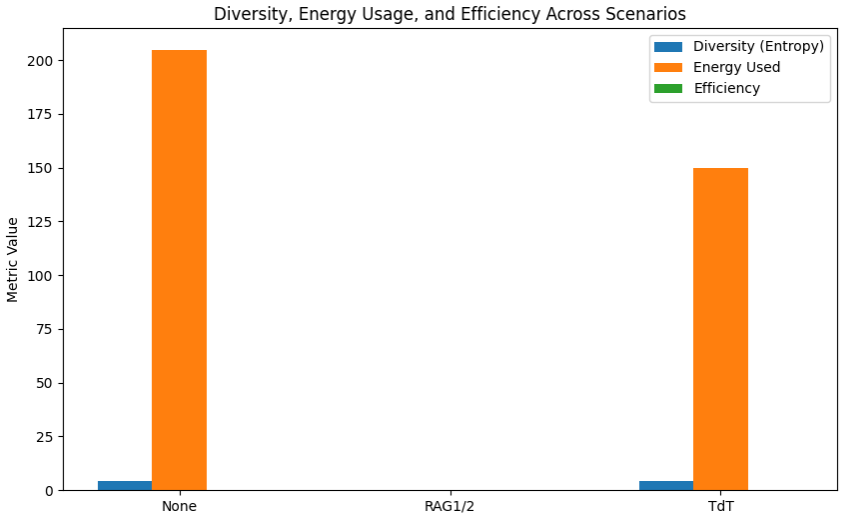

Figure 4: **Receptor Diversity, Total Energy, and Efficiency.** Bars compare the final diversity (blue), the total energy cost (orange), and a derived efficiency metric (green) for each scenario. The highest diversity is achieved in the unperturbed state (left cluster), at the expense of the greatest cumulative cost.

tion balances receptor diversity against metabolic costs, how hierarchical visual processing recovers essential contours under input perturbations, and how agent-based opinion models can form clusters or polarize under local and global forces. Although each domain is unique, the data consistently support the theoretical predictions that memory fosters resilience, partial gating encodes context dependence, feedback stabilizes emergent structures, and thermodynamic costs track the complexity of state reconfiguration.

5.1 Implications of the Figures and Key Observations

One of the strongest confirmations of our framework is the consistency observed across all numerical results, as illustrated in Figures 1–7. For instance, the time-series plots of gene expression (Figure 1, left panels) reveal how a memory-enriched gene regulatory circuit settles into stable attractors across dorsal-ventral coordinates, while the corresponding energy plots (Figure 1, right panels) highlight the initial cost surge that accompanies leaving transient states. Similarly, in our V(D)J recombination simulations (Figure 2, Figure 4), the height of the energy curve correlates with the breadth of the recombined repertoire, suggesting that molecular diversity in adaptive immunity depends on the willingness (or capacity) of a cell to expend nonequilibrium energy. In the hierarchical visual pipeline (Figure 5), side-by-side comparisons of normal and perturbed conditions make it evident that feedback loops can reconstruct coherent images at a measurable metabolic cost. Finally, the opinion-dynamics scenarios (Figure 6 and Figure 7) visually confirm how threshold-based gating and memory can maintain stable clusters, allow occasional flips to synchronize with strong global signals, or produce sustained oscillations across the population.

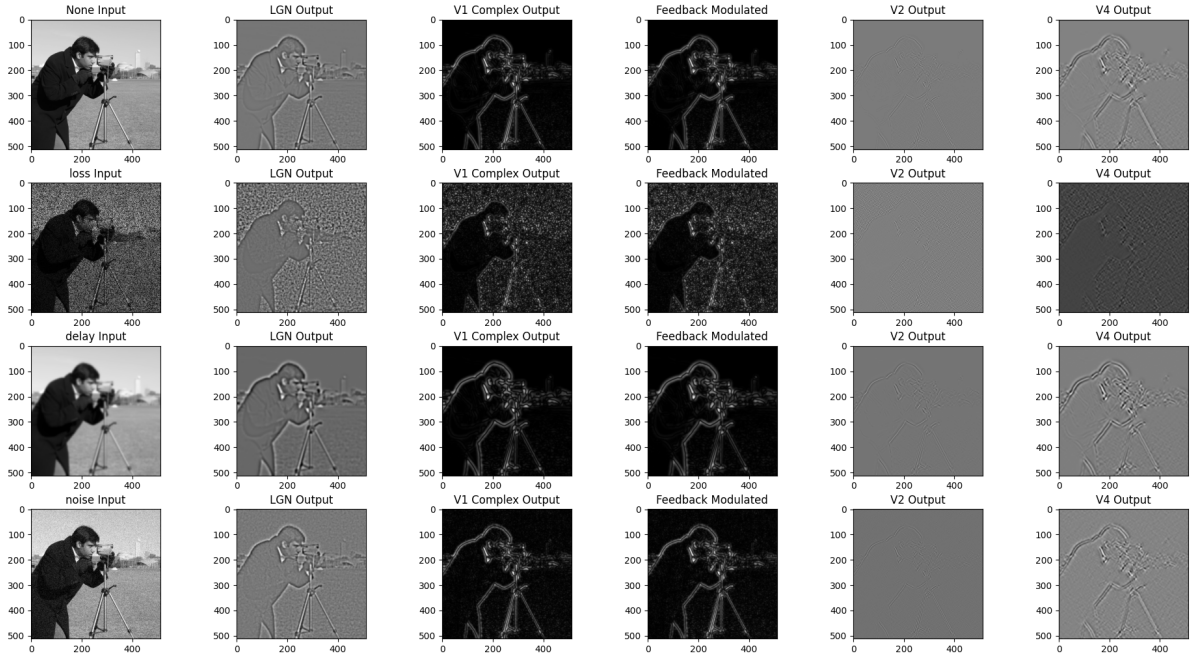

Figure 5: **Hierarchical Visual Processing Pipeline.** Each row corresponds to a distinct perturbation mode (none, partial loss, delay, noise). Columns proceed from raw LGN filtering (left) through V1 Gabor edges, a feedback-modulated stage, V2 texture extraction, and V4 shape pooling. The final V4 outputs recover most salient structures despite upstream corruption, demonstrating that memory-like recurrent loops can offset early deficits at increased energy cost.

These figure-based observations serve as concrete illustrations of our broader theory and provide visual evidence that memory, gating, feedback, and energy constraints act in concert to stabilize or diversify state trajectories. Although each figure focuses on a different biological or social "substrate," the repeated pattern of an early surge in energy usage followed by lower-cost attractor maintenance aligns neatly with the thermodynamic notion that irreversible transformations are most expensive when driving the system away from prior or default configurations.

5.2 Experimental Opportunities for Validating the Framework

A crucial next step is to connect these computational findings with real biological data. Several experimental approaches could validate the core predictions:

- **Gene Regulation and Single-Cell Energetics.** Advanced single-cell sequencing, coupled with live-cell imaging of ATP usage, can measure how early expression changes in embryonic tissues correlate with spikes in metabolic consumption, much like the energy surges we observe in Figure 1. Perturbation experiments where specific genes (e.g., *Pax6*) are knocked out or forcibly overexpressed would reveal whether the sys-

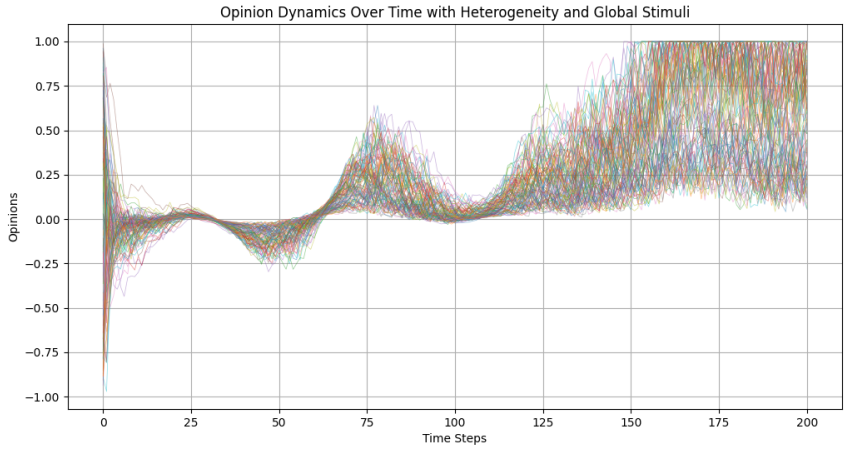

Figure 6: **Temporal Opinion Evolution.** Each line denotes one agent's opinion. The horizontal axis tracks discrete timesteps, and the vertical axis ranges from -1 to 1. Early local clustering is visible by step 50; a global periodic stimulus then aligns or oscillates many agents simultaneously around mid-simulation, increasing cumulative "effort."

tem indeed finds new stable attractors and whether this transition is accompanied by additional resource expenditure.

- **V(D)J Recombination Studies.** By tracking both rearrangement patterns and real-time metabolic indicators in developing B or T lymphocytes, researchers could test whether conditions of higher enzyme activity (RAG1/2, TdT) indeed correlate with elevated cellular energy usage, and whether partial or total knockout recapitulates the predicted drop in receptor diversity and energy consumption. Flow cytometry or single-cell Rep-Seq methods that measure diversity distributions in parallel with metabolic assays would be particularly revealing.

- **Hierarchical Vision in Neural Circuits.** Imaging techniques such as two-photon microscopy or fMRI can track how cortical areas respond under perturbed or noisy stimuli. Specifically, measuring neural firing rates or blood oxygen level signals in both early (LGN, V1) and higher (V4, IT) areas while systematically degrading visual inputs would clarify whether top-down feedback demands additional metabolic resources, mirroring the increased iterative "cost" evident in Figure 5.

- **Collective Opinion Experiments.** Social lab experiments, online forums, or field studies might be designed to detect how a population of agents with memory of past states reacts to threshold-based influences from peers or from an external source (e.g., a media campaign). Surveys or real-time group decision tasks could quantify "effort" (e.g., time or cognitive load) associated with major opinion shifts. Tracking individuals' prior beliefs would help confirm the predicted buffering effects of memory and gating phenomena, as suggested by Figures 6 and 7.

If these empirical tests show that energy usage or "effort" correlates with the predicted

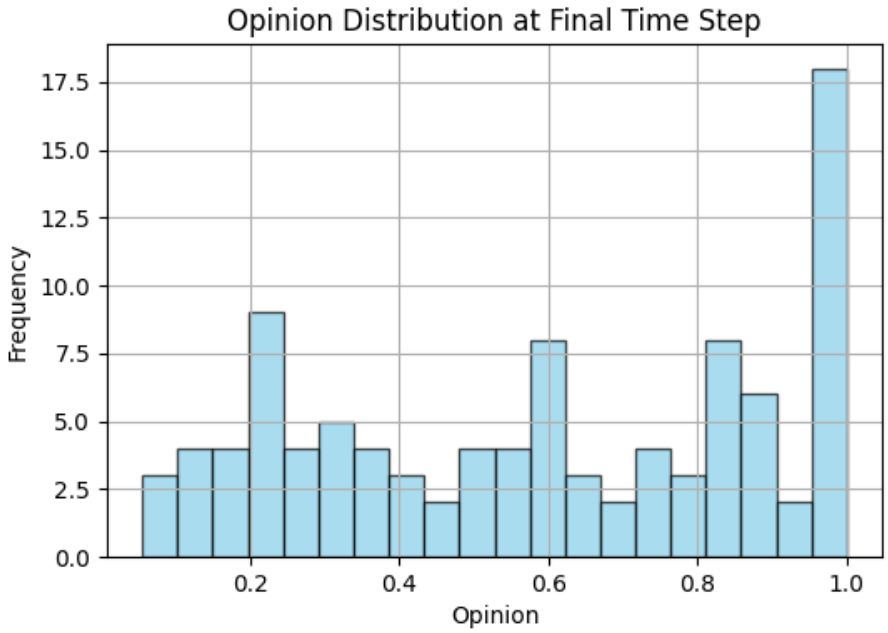

Figure 7: **Final Opinion Distribution.** After 200 steps, agents occupy a limited set of opinion basins. Strong memory/thresholding tends to preserve multiple clusters, whereas weaker gating or potent global stimuli drive near-unanimous convergence.

early surges or threshold-dependent transitions, it would provide significant support for the nonequilibrium principles presented here.

5.3 Further Elaboration on Optimal Transport Connections

Beyond direct experiments, another intriguing avenue for theoretical expansion involves recasting these results in the language of optimal transport. In classical optimal transport, a probability distribution moves over a geometric space along a path that minimizes a certain cost functional, often tied to distances between points and local constraints. In our framework, partial gating can be viewed as imposing high-cost or "closed" edges in the adjacency of state space, while memory kernels effectively alter the distance metric by coupling present transitions to past states. These modifications can make the flow deviate significantly from classical gradient-flow paths.

A fully developed view of this connection might (1) define a discrete metric $d(\mathbf{x}, \mathbf{x}')$ that accounts for gating "barriers," memory expansions, and free-energy differences, (2) rewrite the master equation as a time-discrete or continuous flow in probability space, and (3) compare the system's actual trajectory to a minimal "transport cost" path. In a purely Markovian, detailed-balance-limited scenario, one can interpret the system's evolution as a gradient flow in the Wasserstein metric on a free-energy functional. In our model, partial gating and memory break many of those assumptions, but we can still approximate or bound the nonequilibrium flux in terms of an extended or "piecewise" transport distance. Such expansions could yield novel geometric insights into how gating thresholds produce abrupt

shifts or "folds" in the space of feasible transitions, and how memory extends the dimensionality of effectively navigable states. These ideas might also spur new numerical methods for analyzing large-scale biological or social systems as nonequilibrium flows, bridging the gap between our simulation-based approach and established theoretical tools in transport geometry.

5.4 Limitations and Future Directions

While the core elements of memory, gating, feedback, and thermodynamic costs are successfully demonstrated, several key limitations remain. Our gene regulatory model employs only a 1D approximation of morphogen gradients, omitting 2D or 3D tissue complexities such as mechanical constraints or multicellular contact interactions. The V(D)J simulation abstracts away details of T- or B-cell development and ignores further selective checkpoints that shape the ultimate receptor repertoire. Hierarchical vision, meanwhile, reduces the cortex to only four discrete layers, whereas real neural processing spans numerous interconnected regions with ongoing plasticity. The agent-based opinion model uses relatively simple memory buffers and threshold rules that may not fully capture real-time social adaptation or network inhomogeneities.

Despite these simplifications, the results confirm that each system's computational functionalities are inseparable from their nonequilibrium foundations. Future work might couple these short-term simulations to evolutionary or adaptive timescales, enabling gating thresholds or memory depths to be shaped by selective pressures. More advanced versions of the hierarchical vision pipeline could incorporate lateral connectivity or dynamic synaptic plasticity. And in the domain of social systems, integrating explicit network topologies or agent heterogeneity might yield richer emergent phenomena such as spiral waves of consensus or stable minorities that shift under cyclical external forcing.

5.5 Summary and Outlook

In sum, our simulations and analyses demonstrate that a unifying set of dynamical principles—non-Markovian memory, partial gating, multi-scale feedback, and explicit thermodynamic constraints—can illuminate a broad array of biological computations. The figures, which track state trajectories, cumulative energy usage, and final distributions, illustrate how these principles manifest as stable attractors, trade-offs between diversity and cost, resilient perception under noise, and cohesive or oscillatory opinion clusters. Moreover, the theory's connection to optimal transport suggests a path for deeper mathematical formalization, where gating modifies the geometry of permissible flows and memory adds historical dimensions to the transport problem.

By proposing specific experiments that measure energy consumption, gating thresholds, and memory effects (e.g., single-cell gene expression plus ATP usage, immunological repertoire analysis, neural imaging under degraded stimuli, or opinion shifts in controlled social settings), we emphasize that these ideas are more than abstract constructs: they point toward testable hypotheses about how living systems allocate resources to sustain meaningful computations in nonequilibrium environments. Through further refinement and empirical

validation, we expect this framework to serve as a foundation for investigating how life harnesses physical processes—both historical and conditional—to achieve robust, adaptable, and irreversibly transformative computations across scales.

6 Conclusion

This study has demonstrated how four seemingly disparate biological processes—gene regulation, immune segment recombination, hierarchical vision, and opinion formation—can all be interpreted within a common theoretical framework incorporating memory, partial gating, hierarchical feedback, and explicit thermodynamic costs. By evaluating the data from each simulation (Figures 1–7), we have shown that each domain expresses analogous patterns of robust attractors, conditional transitions, multi-level control, and energetic trade-offs. These parallels highlight the potential to unify diverse biological computations as nonequilibrium flows through state space, shaped by enabling conditions and carried by memory-dependent fluxes.

Though the present models remain simplified and do not exhaustively capture real-world complexities, they offer a generative framework that can be refined to address spatial heterogeneity, adaptive gating, or evolutionary processes. They also point to deeper connections with geometric treatments of probability flows, particularly where partial gating and memory might be reframed as constraints or expansions within an optimal transport setting. From a practical standpoint, we anticipate that quantitative measurements of energy usage, gating thresholds, and memory traces in living systems will become increasingly feasible through single-cell imaging, advanced neuroimaging, and data-rich social platforms. Such evidence can validate or refine this thermodynamically consistent view of biological computation, helping us understand how life orchestrates conditional transformations to maintain function, diversity, and stability under perpetual nonequilibrium conditions.